


Research Article

A New Dynamic Balance Framework Based on Blind Source Separation under Multiple Fault Conditions

Bo Lang,¹ Xinyi Zhang,¹ Jun Xiao,² Shouhang Lu,³ and Bing Li ^{4,5}

¹School of Mechanical Engineering, Xi'an Jiaotong University, Xi'an, Shaanxi 710049, China

²State Key Laboratory of Compressor Technology (Anhui Laboratory of Compressor Technology), Hefei, Anhui 230031, China

³Xi'an Shaangu Engineering and Technology Co., Ltd, Xi'an, Shaanxi 710075, China

⁴School of Mechano-Electronic Engineering Xidian University, Xi'an, Shaanxi 710071, China

⁵Xi'an Key Laboratory of Intelligent Instrument and Packaging Test, Xidian University, Xi'an, Shaanxi 710071, China

Correspondence should be addressed to Bing Li; libing@xidian.edu.cn

Received 17 June 2022; Revised 8 August 2022; Accepted 9 August 2022; Published 29 September 2022

Academic Editor: Liu Jing

Copyright © 2022 Bo Lang et al. This is an open access article distributed under the Creative Commons Attribution License, which permits unrestricted use, distribution, and reproduction in any medium, provided the original work is properly cited.

Accordingly, the mass unbalance of the rotors is usually the major cause of excessive vibration. The information extracted at the fundamental frequency is often employed to fix the unbalance issue. However, other rotor faults like rotor bending and bearing-failure effect also generate additional components to the characteristics. Thus, it is necessary to isolate the corresponding features and obtain the intrinsic causes of the multiple failures. In this paper, a productive hybrid method is successfully developed to deal with the root mass unbalance problem with additional force interference by integrating the superiority of different methods, including Ensemble Empirical Mode Decomposition (EEMD) and Nonnegative Matrix Factorization (NMF), where EEMD is used to obtain sensitive IMFs and NMF is employed to acquire the inherent source signal, respectively. Meanwhile, a root dynamic balancing and implemental framework is also developed to accomplish the task of vibration reduction. For verification, a serial of simulations and experimental investigations have been analysed to demonstrate the preferable potentialities of the proposed method. In particular, a standard Bently Nevada rotor rig with a specifically designed device was employed to simulate appended faults by adjusting the additional forces during the experimental steps. The analysis results show that the proposed method can isolate and extract the unbalance faults from the raw vibration signals and achieve accurate correction balancers, where a nearly identical correction angle has been achieved, which indicates that the optimal installation position has been successfully figured out.

1. Introduction

As one of the most vital apparatuses, rotating machinery of great significance in defensive and civil fields is the fundamental infrastructure and key to national economic production equipment. Unfortunately, these oscillatory systems are easily susceptible to unwanted vibrations, where some negatives and factors like excessive vibration, structural noise, and thermal deformation will be generated and significantly enhanced with the increase of rotational speed [1–4].

In reality, a rotor system may suffer from different types of failures during long-term operating. The most common

causes including unbalance, misalignment, fatigue crack, thermal deformation, rotor-stator friction, and bending may further induce sudden breakdowns and make undesired vibrations arise during operation [3–5]. Among the abovementioned causes, unbalance failures represent 35% of the mechanical problems of rotating machines and account for more than 75% of the rotating machine vibration fault [1, 6, 7]. Therefore, it is critical and reasonable to investigate effective and reliable techniques to eradicate this issue and further achieve reliable operation.

In addition, it is cumbersome to fix the mass unbalance issue under multifault condition, in which another aspect of the rotor system vibration behaviour can also be traced to

initial deformations like rotor bending and contact friction. In particular, the coupling misalignment and the thermal bowing can also change the unbalance distribution [8]. Once the preliminary deformation of a rotor shaft couples with the unbalance issue, the synchronous vibration response, which only differs from the mass unbalance, can be extracted [9]. In this case, the characteristics extracted from analysis sources like vibration and acoustics become ambiguous and unintuitive. Thus, to identify and isolate the inherent features that directly reflect the rotor faults and achieve reliable maintenance strategies and practical operations, more effective and in-depth investigations should be established to address the above issues.

Nowadays, lots of literature has accumulated and documented many investigations on rotor systems such as base motion, vibration resonance, friction, and contact [10]. In particular, in situ rotor balancing has attracted considerable attention from industry and academia [3, 11–13]. Meanwhile, the research and development on the efficient dynamic balancing method have been treated as a decisive technology for fault recovery and vibration reduction [10]. Specifically, representative methods used to address the rotor unbalance issue involve the influence coefficient method (ICM), modal balancing, Holo-balancing, and autobalancing [2, 10, 14–17]. As a data-driven method, ICM that only requires machine runs with trial weights can be simply implemented without any prior knowledge of the rotor model. ICM has been widely employed and intensively applied in the industry and experimental environment, and the corresponding theory and applications are matured after years of development and refinement [15]. On the other hand, if the full-model parameters of the rotor system are known in advance, the modal balancing method can be highly competent to account for rotor unbalance using the modal shapes. In this method, the intrinsic mechanism relies heavily on adding trial weights to N balance surfaces to counteract the corresponding N modal unbalance responses [10, 15]. Generally, to achieve a satisfactory result using modal balancing, one should rely on an accurate numerical model and prior knowledge of the entire rotor dynamics or a highly skilled engineer. As for the Automatic Ball Balancer (ABB), it can be used to reduce rotor vibrations by compensating for mass unbalance of the rotor. This method is better adapted to applications where the amount of imbalance varies with the operating conditions. However, due to its inherent nonlinear properties, on some occasions, especially during the run-up and shutdown stage, ABB may enhance the original vibration level rather than eliminating the vibration response [17]. Owing to the advantages of easy implementation and high efficiency, ICM has become the most commonly used balancing method in industries.

In general, the vibration frequencies of the rotor imbalance are synchronous, i.e., one times the shaft rotational speed (1X rpm), and the imbalance forces cause the shaft rotation frequency (1X) dominating its harmonic frequencies [18]. The core issue of the dynamic balancing procedure is to precisely extract the 1X frequency components from the raw vibration signal. However, it could be a daunting task to obtain the pure unbalance components of 1X, especially for

multiple faults, since other rotor failures such as cracks, bends, looseness problems, and misalignments also introduce disturbances to the balancing characteristics of the rotor system [2, 3, 19]. That is, the evidence 1X commonly calculated from the original signal should be treated as the superposition of different frequency responses that are closely associated with the external forces generated by the rotor failure. In field operations, however, many technicians indiscriminately use the mixed amplitude and phase information at 1X to handle the mass unbalance without considering the superposition of unbalance and other rotor faults. Sometimes, promised results may be achieved with the entire vibration level decreasing to the allowable range or even better. However, vibration symptoms may reappear or even increase within a short period of time once the fault coupling force changes, i.e., oil-film force and blade force. The reason for the phenomenon is briefly induced by the root cause misjudgment. Thus, fault coupling and isolation procedures should be on the agenda and systematically investigated to reach the root response characteristics and further improve the maintenance effect.

In this paper, we focus on identifying the inherent unbalance parameters of the rotor system using blind source separation (BSS) and Ensemble Empirical Mode Decomposition under multiple fault conditions. The two signal processing methods are introduced in Section 2. As a representative and prevalent BSS technique, Nonnegative Matrix Factorization (NMF) is delivered to accomplish the fault isolation task. EEMD is employed to calculate the most valuable intrinsic mode functions (IMFs). Thereafter, the fundamental principle of ICM is described and the main framework of the proposed method is illustrated. The effectiveness of the new method is verified using different simulations and experiments, and some relevant discussions are presented in the next section. Finally, some conclusions are presented in the last section.

2. Basic Concepts of the Involved Signal Processing Approaches

To figure out the root response that corresponds to the inherent fault, in the current section, a new fusion approach is established by combining Ensemble Empirical Mode Decomposition (EEMD) with Nonnegative Matrix Factorization (NMF) to accomplish the ultimate target of inherent unbalance extraction. The principles of the two methods are briefly introduced. Thereafter, the core framework is given.

2.1. Nonnegative Matrix Factorization. Blind source separation (BSS) is widely used to extract underlying information from a mixture of different behaviours, i.e., multifault response and mixed sound signals. The main task of BSS for signal decomposition relies on inferring and estimating the most probable sources [20], i.e., fault signals and speech components from the acquired signals. The ideal model of BSS can be formulated as

$$\mathbf{X}(t) = \mathbf{A}\mathbf{S}(t) + \mathbf{E}, \quad (1)$$

where $\mathbf{X}(\mathbf{t}) \in \mathbf{R}^{P \times N}$ is the so-called observed matrix that can be expressed as $[x_1(t), x_2(t) \cdots x_p(t)]^T$; $\mathbf{S}(\mathbf{t}) \in \mathbf{R}^{n \times N}$ is the separated matrix that consists of unknown source signals, i.e., $\mathbf{S}(\mathbf{t}) = [s_1(t), s_2(t), \cdots s_n(t)]^T$; $\mathbf{A} \in \mathbf{R}^{P \times n}$ stands for the mixing matrix and $\mathbf{E} \in \mathbf{R}^{P \times N}$ denotes the additive Gaussian noise with zero mean.

Unlike most BSS algorithms that learn holistic representations, e.g., independent component analysis (ICA), principal component analysis (PCA), and sparse component analysis (SCA), Nonnegative Matrix Factorization (NMF) only learns partial features with nonnegative constraints to better decompose the objective matrix. The output of NMF is to figure out an approximate factorization into two nonnegative factors. Since NMF was first proposed by Lee and Seung in nature, it has attracted widespread interest at the intersection of many scientific and engineering disciplines, such as face recognition, blind source separation, speech enhancement, fault diagnosis, pattern recognition, and data mining [21, 22].

Given a matrix \mathbf{V} with nonnegative observations v_{ij} , NMF is used to factorize matrix \mathbf{V} into two main parts: the basis matrix \mathbf{W} and component matrix.

$$\mathbf{V} \approx \mathbf{W}\mathbf{H}$$

$$s.t. v_{ij} \geq 0, w_{ik} \geq 0, h_{kj} \geq 0, i = 1, \dots, n; j = 1, \dots, m; k = 1, \dots, r \quad (2)$$

where $\mathbf{V} \in \mathbf{R}^{n \times m}$ is a nonnegative mixed matrix constructed and formed from vibration vectors, $\mathbf{W} \in \mathbf{R}^{n \times k}$ is the basis matrix that is considered as a set of basis vectors, and $\mathbf{H} \in \mathbf{R}^{k \times m}$ is so-called coefficient matrix (or component matrix) that is treated as the coordinates of each sample with respect to these basis vectors [22, 23].

To accomplish the factorization of $\mathbf{V} \approx \mathbf{W}\mathbf{H}$ as accurately as possible, a robust and effective objective function should be designed to quantify the approximation quality. Herein, the commonly used squared error (Euclidean distance) function and the Kullback–Leibler divergence are introduced as the objective functions for factorization.

The objective function of NMF is formulated by the Euclidean distance; namely,

$$D(\mathbf{V} \parallel \mathbf{W}, \mathbf{H}) = \|\mathbf{V} - \mathbf{W}\mathbf{H}\|^2 = \sum_{i,j} [v_{ij} - (\mathbf{W}\mathbf{H})_{i,j}]^2 \quad (3)$$

$$s.t. \mathbf{W}_{ia} \geq 0, \mathbf{H}_{bj} \geq 0, \forall a, b, i, j$$

where $D(\mathbf{V} \parallel \mathbf{W}, \mathbf{H})$ stands for the distance between the data matrix and the two factorized matrixes.

Correspondingly, the objective function constructed in terms of Kullback–Leibler divergence is given as follows:

$$\min D(\mathbf{V} \parallel \mathbf{W}, \mathbf{H}) = \sum_{i,j} \left\{ v_{ij} \left[\log \left(\frac{v_{ij}}{(\mathbf{W}\mathbf{H})_{i,j}} \right) - 1 \right] + (\mathbf{W}\mathbf{H})_{i,j} \right\} \quad (4)$$

$$s.t. \mathbf{W}_{ia} \geq 0, \mathbf{H}_{bj} \geq 0, \forall a, b, i, j$$

As can be noticed in (4), the core values of NMF can be recognized as the optimal linear combination using the basis matrix to approximately recover the original data matrix.

The objective function of the NMF optimization model based on Euclidean distance is a bit simpler to implement and achieve good performance.

Theoretically, it is scarcely possible to find the global minima of the objective function, since the convexification of the two terms (\mathbf{W}, \mathbf{H}) together could be a long-beleaguered task. To minimize the cost function, Lee and Seung presented efficient multiplicative elementwise update formulae for these two minimization problems and proved their convergence [22, 23].

The alternation and iterative operations are utilized for matrix updating, i.e., the n th updated result $\mathbf{W}^{(n)}$ is fixed and employed for the further renewable process on $\mathbf{H}^{(n+1)}$. Thereafter, a new iterative result $\mathbf{W}^{(n+1)}$ can be calculated using the unvaried item $\mathbf{H}^{(n+1)}$. The regeneration formulae for the Euclidean distance are written as

$$\left\{ \begin{array}{l} w_{ik} \leftarrow w_{ik} \frac{(\mathbf{V}\mathbf{H}^T)_{ik}}{(\mathbf{W}\mathbf{H}\mathbf{H}^T)_{ik}} \\ \\ h_{kj} \leftarrow h_{kj} \frac{(\mathbf{W}^T\mathbf{V})_{kj}}{(\mathbf{W}^T\mathbf{W}\mathbf{H})_{kj}} \end{array} \right. \quad (5)$$

For the Kullback–Leibler divergence model, the corresponding updated role is

$$\left\{ \begin{array}{l} w_{ik} \leftarrow w_{ik} \frac{\sum_j h_{kj} v_{ij} / (\mathbf{W}\mathbf{H})_{ij}}{\sum_u h_{ku}} \\ \\ h_{kj} \leftarrow h_{kj} \frac{\sum_i h_{ik} v_{ij} / (\mathbf{W}\mathbf{H})_{ij}}{\sum_v h_{vk}} \end{array} \right. \quad (6)$$

The steady states of the two matrices \mathbf{W} and \mathbf{H} can be achieved and the iteration is terminated when the iteration number of NMF algorithm reaches its threshold. More details can be found in [21, 23].

For source separation or dimension reduction, the number of rows r is supposed to satisfy the inequality $r(m+n) < mn$. Note that the key parameter r is related to the expected number of faults in the rotor system in our following application.

2.2. Ensemble Empirical Mode Decomposition. Empirical Mode Decomposition (EMD) method has attracted considerable attention and has been widely investigated in the

fields of condition monitoring and fault diagnosis. EMD-based research and application have become an important branch for handling nonlinear and nonstationary data. This technique can decompose the analysis signal into a serial of intrinsic mode functions (IMFs) or monocomponent functions. Meanwhile, each IMF satisfies the following prerequisites and definitions [24–26].

Firstly, in the whole data set, the number of extrema and the number of zero-crossings must be equal or differ by at most one.

Secondly, at any point, the mean value of the envelope defined by the local maxima and the envelope defined by the local minima must be equal to zero.

Through the standard procedure, the final decomposition result can be gained accordingly.

$$\mathbf{Y}(t) = \sum_{i=1}^n \mathbf{c}_i(t) + \mathbf{r}_n(t). \quad (7)$$

According to the theory of EMD, the relevant center frequency for each IMF component gradually reduces, where the first IMF owns the highest frequency bandwidth while the last IMF is associated with the low-frequency components. Conventionally, for the sake of fault diagnosis, the usual practice relies on the features extraction from the first few IMFs since localized fault characteristics are usually displayed in the high-frequency bands. However, as for further information utilization, different IMF components have abilities in which the discarded low-frequency IMFs may contain beneficial effects that can be further utilized to treat other applications.

EMD also suffers from several inherent drawbacks, i.e., the choice of a relevant stopping criterion, mode-mixing problem. Mode-mixing that can be arbitrarily split into two groups, including oscillations of dramatically disparate scales and similarly scaled components residing in different IMFs, is the major drawback of EMD, sometimes causing severe aliasing or inducing unpredictable and inexplicable results.

By means of adding a finite white noise to the raw signal, EEMD was successfully developed to improve the EMD algorithm [26, 27]. It can be seen that EEMD is a noise-assisted data analysis method. Here, the two parameters, the ensemble number and the noise level, play an important role in determining the decomposition effect. Some background theories and applications can be found in [25, 27]. The corresponding flow of EEMD can be briefly listed as follows.

Step1 Collect the original noise signal $\mathbf{Z}(t)$ from the experiment platform or field industry.

Step2 Set the initial parameters of the noise components and the number of ensemble M .

Step3 Construct loops for each IMF extraction and perform M times of standard EMD steps for the signal with white noise while the loop is repeated.

Step4 Calculate the ensemble average of M trials to obtain the related IMFs during this loop.

Step5 Compute the residual $R_m(t) = \mathbf{Z}(t) - \text{IMF}_i(t)$.

Step6 Consider the residual signal as the original signal and repeat the whole process until a constant residual is achieved.

If necessary, it is suggested for the reader to view [25] for more details of EEMD algorithm.

2.3. Brief Summary of Rotor Balancing. The influence coefficient, which can reflect the linear relationship between the trial weight and characteristics, is relevant to the sensor/balancer position and the rotating speed (see Figure 1).

Once the trial weight is installed into the correction plane, the characteristic response of 1X from the output end is obtained. The influence coefficient in Figure 1 briefly relies on two assumptions: (1) the rotor synchronous response is proportional to the imbalance; (2) the effects of individual imbalances can be superimposed to obtain the effect of a set of imbalances [19, 28].

The general formulation of the influence coefficient method is

$$\mathbf{V} = \mathbf{V}_0 + \mathbf{P}\mathbf{D}, \quad (8)$$

where $\mathbf{V} \in \mathbf{C}^{r \times 1}$ is the complex vector representing the rotor synchronous vibration (1X) measured at r locations, $\mathbf{V}_0 \in \mathbf{C}^{r \times 1}$ denotes the synchronous vibration at the r sensor position caused by the system inherent imbalance, $\mathbf{P} \in \mathbf{C}^{r \times s}$ is the influence coefficients matrix, and $\mathbf{D} \in \mathbf{C}^{s \times 1}$ is the imbalance weight provided by the balancer in the balancer coordinate system.

The matrix \mathbf{P} can be obtained after a series of trial runs. Assume that the vibration characteristic is V_i when the imbalance of the balancer D_i is installed into the correction plane. Then, the influence coefficient is estimated using (2)

$$P^{ij} = \frac{V_1^i - V_2^i}{D_1^j - D_2^j}, \quad (9)$$

where P^{ij} is the ij th element of \mathbf{P} , V^i represents the vibration at the i th measurement location, and D^j is the imbalance provided by the j th balancer.

The optimal imbalance weights can be obtained using the least squares solution:

$$\mathbf{D} = -(\mathbf{P}^T \mathbf{P})^{-1} \mathbf{P}^T \mathbf{V}_0. \quad (10)$$

For more detailed information about ICM, the readers can be referred to [19, 28].

2.4. The Proposed Procedure for Dynamic Rotor Balance. With the assistance of NMF and EEMD, a hybrid method named BSS-ICM is developed to accomplish the multiple fault identification and isolation tasks. Meanwhile, a root dynamic balancing and implemental framework is also proposed to realize vibration reduction, in which the main goal is to find the root inherent balancing causes and to further operate with safety, stability, and long-term runnings.

The sketch of the proposed main framework can be seen in Figure 2.

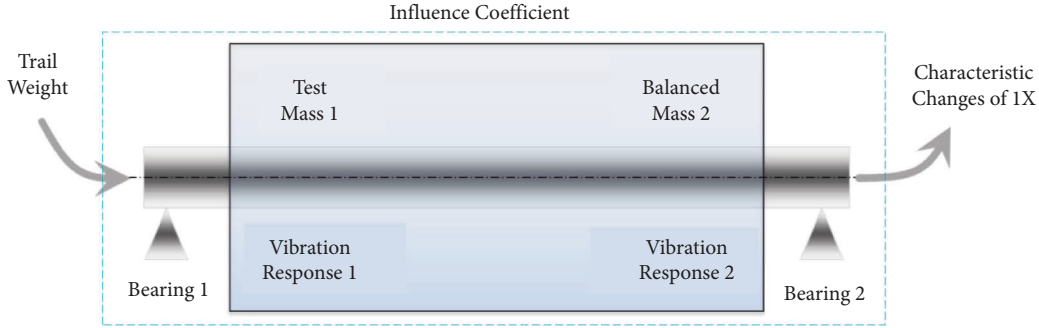


FIGURE 1: The influence coefficient calculation model.

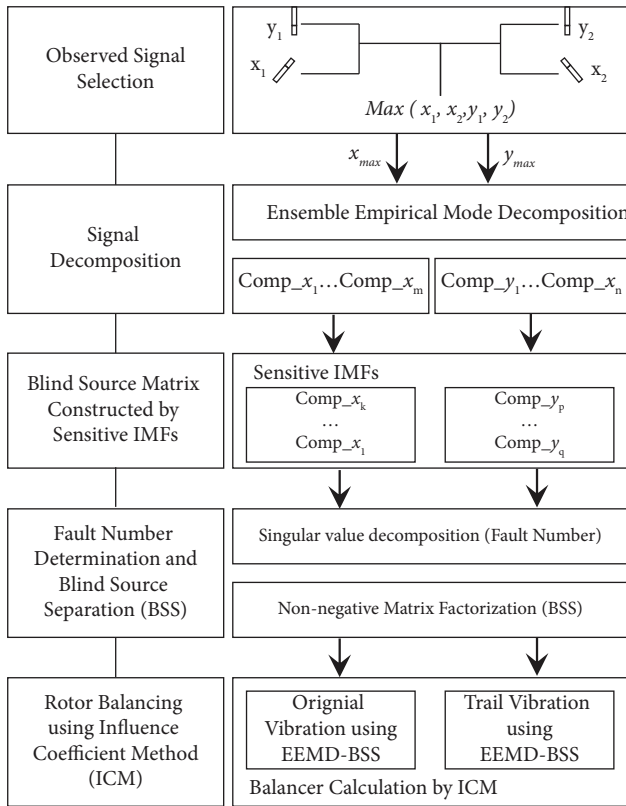


FIGURE 2: The framework of BSS-ICM.

As can be viewed in Figure 2, the new method mainly consists of five portions, i.e., observed signal selection, signal decomposition, blind source matrix construction, fault number determination, blind source separation, and ICM-based rotor balancing.

- (1) Signal collection and analysis source selection: the observed signal is simultaneously collected by the acquisition system and selected for further analysis according to the magnitude level. Note that the comparison must be applied to signals of the same direction.
- (2) Signal decomposition: EEMD is utilized to decompose each selected signal into a serial of IMFs. Sensitive IMFs are identified according to the

similarity between the extracted IMF and the original signal. The basic idea of IMF selection relies on the use of representative IMFs to replace the raw signal for precise balancing calculation.

Herein, the cosine similarity measure metric is involved in enhancing the effectiveness and automation of IMF selection. This metric is originally defined as the inner product of two vectors $\mathbf{X} = [x_1, x_2, \dots, x_N]$ and $\mathbf{Y} = [y_1, y_2, \dots, y_N]$ divided by the product of their lengths [24], which can be written as

$$\begin{aligned} \text{Sim}_{\cos}(\mathbf{X}, \mathbf{Y}) &= \cos(\alpha) \\ &= \frac{|\sum_{k=1}^N x_k y_k|}{\sqrt{\sum_{k=1}^N x_k^2} \times \sqrt{\sum_{k=1}^N y_k^2}} \end{aligned} \quad (11)$$

Note that the symbol α in (11) represents the included angle between the two vectors. Herein, we a little more focus on the cosine similarities than the angle itself. It can be observed that the magnitude range of the similarity starts from [0, 1], where the more extensive the cosine value is, the higher the similar degree of two vectors would be and vice versa.

- (3) Blind source matrix construction: the source matrix is constructed using the sensitive IMFs. The popular Singular Value Decomposition (SVD) is employed to calculate the fault number in the rotor system. Number estimation is considered as a crucial step in most BSS circumstances. The main principle behind this strategy is that the dominant and nondominant singular values obtained by SVD correspond to the faulty and normal component, respectively. Thus, the largest decline ratio of adjacent eigenvalues can be delivered as a criterion to distinguish the faults from normal (or noise).
- (4) Nonnegative matrix factorization is utilized to decompose the source matrix to acquire the inherent source signal.
- (5) Depending on the signal characteristics, fault diagnosis and isolation results can be demonstrated from

the inherent source signal. Signals with dominated amplitudes at 1X and very small amplitudes at other harmonics will be treated as the vibration responses related to the mass unbalance failure.

- (6) ICM is introduced to accomplish the balancing task once the original and the trial signals are processed using the above steps.

3. Case Studies for Performance Verification

To evaluate the performance of the proposed approach, in this section, different verifications using simulations and experiments have been concerned and demonstrated by means of BSS-ICM. Note that all simulations and experiments were performed on a computer with the Intel Core i7-8565u@1.80 GHz 1.99 GHz and 16.0 GB (15.7 GB usable) memory by 64 bit MATLAB 2010b on Windows 10.

3.1. The Main Comparison Flowchart. To make a systematic comparison, three groups of analyses are involved in this section. The main comparison flowchart is shown in Figure 3. For illustration purposes, the studies related to these three groups are named case 1 (conventional ICM without other faults), case 2 (conventional ICM with additional force), and case 3 (BSS-ICM with additional force).

According to Figure 3, some important descriptions are briefly given.

- (1) Conventional ICM is employed to address the rotor balancing issue under different conditions, i.e., with and without other failures. In this case, the balancing parameters calculation of the rotor system without other faults is regarded as the reference.
- (2) Without regard to the distinction between the two methods (conventional ICM and BSS-ICM), the whole signal comparison process is quite similar, using the same signals and obtained results with the same patterns.
- (3) Since it is quite difficult to simulate the whole process of rotor balancing, the final step in Subsection 3.3 using ICM is abruptly neglected in the simulation case. Analysis results from the first five steps of BSS-ICM will be used to validate the operating performance in this case.
- (4) For a common and united comparison, the simulation and experimental parameters are identically designed (see Table 1).

Note that, due to the space restraint, the rotor system without fault using BSS-ICM is ignored in the experimental case in Section 3.3.

3.2. Numerical Simulations and Discussions. In this section, numerical simulation is introduced to verify the performance of the proposed algorithm. The effectiveness of BSS-ICM is validated by comparing the extraction results with the simulated sinusoidal signal that only contains one frequency component. The single frequency signal herein

denotes the vibration response generated by the mass unbalance.

The two-fault candidate can be considered as one of the most prevalent and representative multiple fault patterns in industrial applications, and multiple faults with more than two sources rarely occur due to periodical maintenance and scientific management. Thus, the mixed signal containing two sources is employed to highlight the prominent properties of our method.

Let \mathbf{Q} be the observed matrix composed of a white noise term $v_i(t)$ and a superposition of two sources, i.e., $S_1(t)$ and $S_2(t)$. The source and mixed signals are defined as follows, respectively:

$$\begin{cases} s_1(t) = d_1 \sin(2\pi f_1 t + \varphi_1) + v_1(t) \\ s_2(t) = d_2 [1 + \sin(2\pi f_1 t + \varphi_2)] \sin(2\pi f_2 t + \varphi_4) + v_2(t)' \end{cases} \quad (12)$$

$$\mathbf{Q} = \begin{bmatrix} Q_1(t) \\ Q_2(t) \end{bmatrix} = \mathbf{A}\mathbf{S} = \begin{bmatrix} a_{11} & a_{12} \\ a_{21} & a_{22} \end{bmatrix} \begin{bmatrix} s_1(t) \\ s_2(t) \end{bmatrix}, \quad (13)$$

where the corresponding parameters are illustrated in Table 2.

During the simulating process, the mixing matrix \mathbf{A} is artificially designed as

$$\mathbf{A} = \begin{bmatrix} a_{11} & a_{12} \\ a_{21} & a_{22} \end{bmatrix} = \begin{bmatrix} 0.8 & 0.6 \\ -0.7 & 0.1 \end{bmatrix}. \quad (14)$$

The signal is generated over a time of 0.5 s with a sample frequency of 1 kHz. Figure 4 gives two time curves of the observed signals $Q_1(t)$ and $Q_2(t)$. EEMD results related to $Q_1(t)$ are shown in Figure 5.

Meanwhile, the cosine similarities between each IMF and the observed signals are obtained by (11) and listed in Tables 3 and 4, respectively. The IMF with the most prominent similarity is selected to achieve the source separation task, while the others are discarded as irrelevant components. Here, IMF3 and IMF2 are, respectively, selected and utilized for further analysis as they own the highest similarities compared to the others in each table.

By comparing the observed signal in Figure 4(b) with its IMFs in Figure 5, significant evidence can be automatically obtained and visually distinguished.

Thereafter, SVD is delivered to estimate the source number and the first 20 decline ratios are plotted in Figure 6.

It can be noticed that the highest value of the decline ratio shows up at the second position, which means that the source number is equal to two accordingly.

Thereafter, the observed matrix and the selected IMFs are treated as the new observed matrix and processed using the NMF method to carry out the inherent sources. Furthermore, to reflect the original sources \mathbf{S} , i.e., $s_j(t)$ and $s_2(t)$, the extracted sources are estimated by the characteristics of frequency distribution. For better comparison, the corresponding components for the same pattern are intensively drawn in the single chart in Figure 7.

At first glance, analogous properties appear in each chart in Figure 7, especially the phase information, where nearly identical results have been achieved. On closer inspection, a

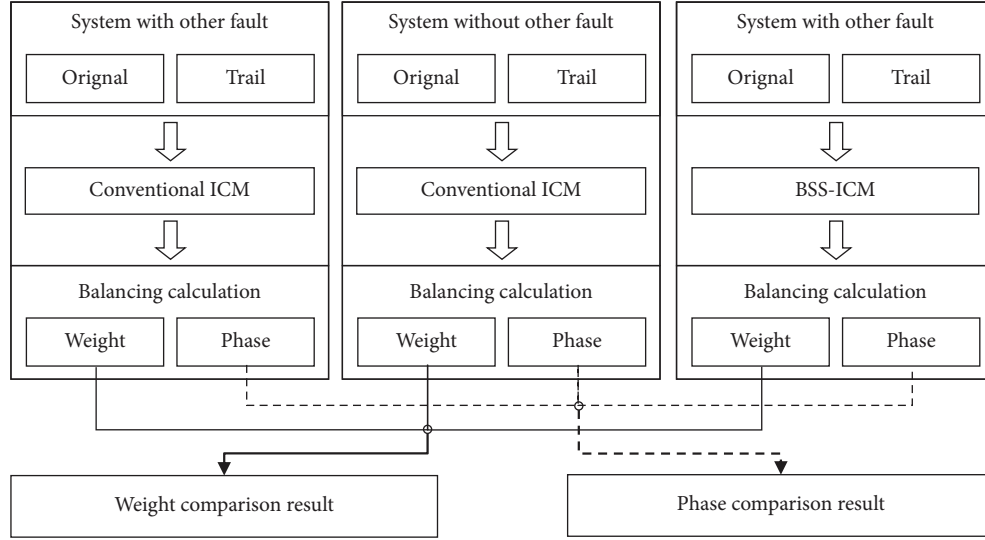


FIGURE 3: The main comparison flowchart using the proposed method.

TABLE 1: Same parameters used for simulation and experiment cases.

Parameters	Source number	Sensitive IMFs number	Ensemble number	Noise level	Max iterative	Residual threshold
Values	2	2	100	0.1	10000	1e-5

TABLE 2: Some parameters of the mixed signal in (12).

Parameters/units	$d_1/\mu\text{m}$	f_1/Hz	φ_1/rad	$d_2/\mu\text{m}$	φ_2/rad	f_2/Hz	φ_3/rad	$v_i(t)$
Values	20	20	$\pi/3$	15	$\pi/4$	40	$\pi/2$	10 dB

slight difference can be noticed between these two charts. In Figure 7(a), for the simulated mass unbalance components, the estimated amplitudes coincide precisely with each other, and a tiny phase shift phenomenon shows up. In Figure 7(b), the fluctuation has increased between the theoretical and the estimated sources. However, the phase shift seems disappeared compared to the previous case. Note that the difference between the theoretical and estimated sources in each case is so slight that the spectrum calculation and analysis are negligible considering the space limitation.

It can be inferred from the above discussions that the extracted information corresponding to the “mass unbalance” obtained by the proposed method is perfectly reserved and can be representatively used for further unbalancing calculations.

3.3. Experimental Results and Discussions

3.3.1. Experiment Setup. To verify the rotor balancing performance in practice, a series of experiments are developed under different external forces. Note that multiple faults are simulated using a specifically designed Bently Nevada Rotor Kit (see Figure 8).

Figure 8 illustrates the structure chart of the rotor balancing test rig together with the specific loading structure. As can be observed, the whole rig consists of a speed controller, a DC motor, a serial of standard weights, and a small range electric balance. A NI-4432 data acquisition card was used for the vibration signal collection. Moreover, six eddy current displacement probes perpendicular to each other were installed separately and further used to perform the task of vibration information capture (see Figure 8(a)). The other two probes were employed for speed measurement and control. More details of the rig can be found in [19].

It needs to be emphasized that the specific loading device installed is used to simulate additional failures like pipeline excitation, which directly affect the distribution of the radial forces by the four linked springs (see B-direction in Figure 8(a)). The current device is able to generate different levels of external forces in terms of the four round nuts. Theoretically, it is capable of loading radial forces in any direction on the rotating components. Since the force applied to the spring is proportional to the spring deformation, the change of the deformation can be quantified and transformed into the changes of pitch number. Thus, the pitch number directly substitutes the real force for convenience.

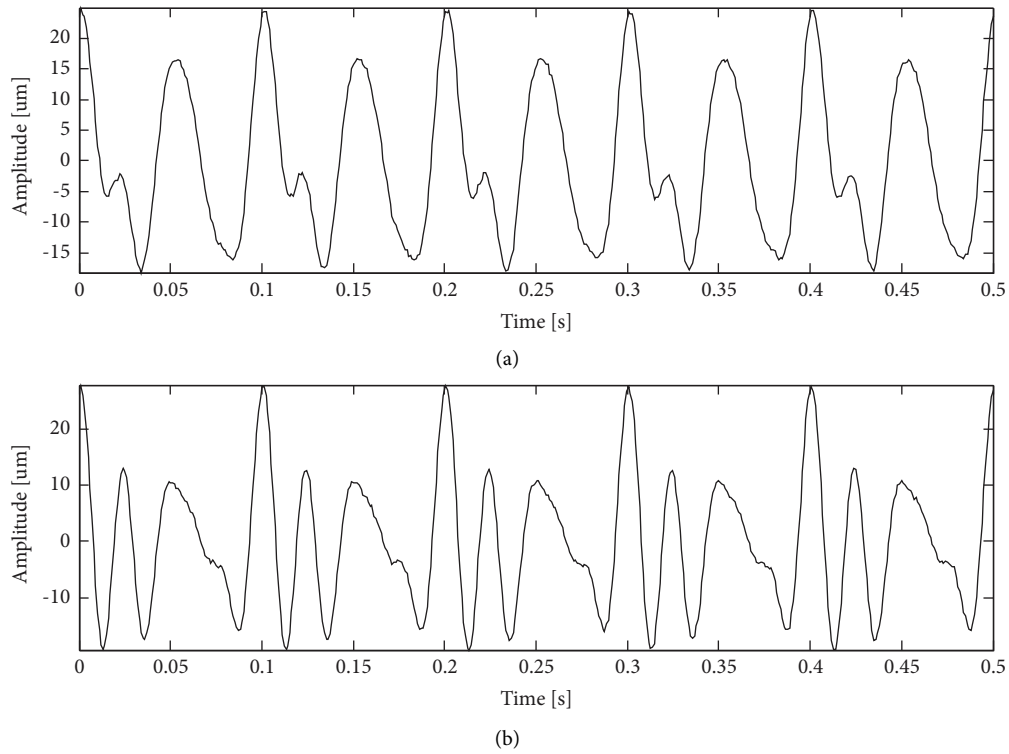


FIGURE 4: Time curves corresponding to the two observed signals.

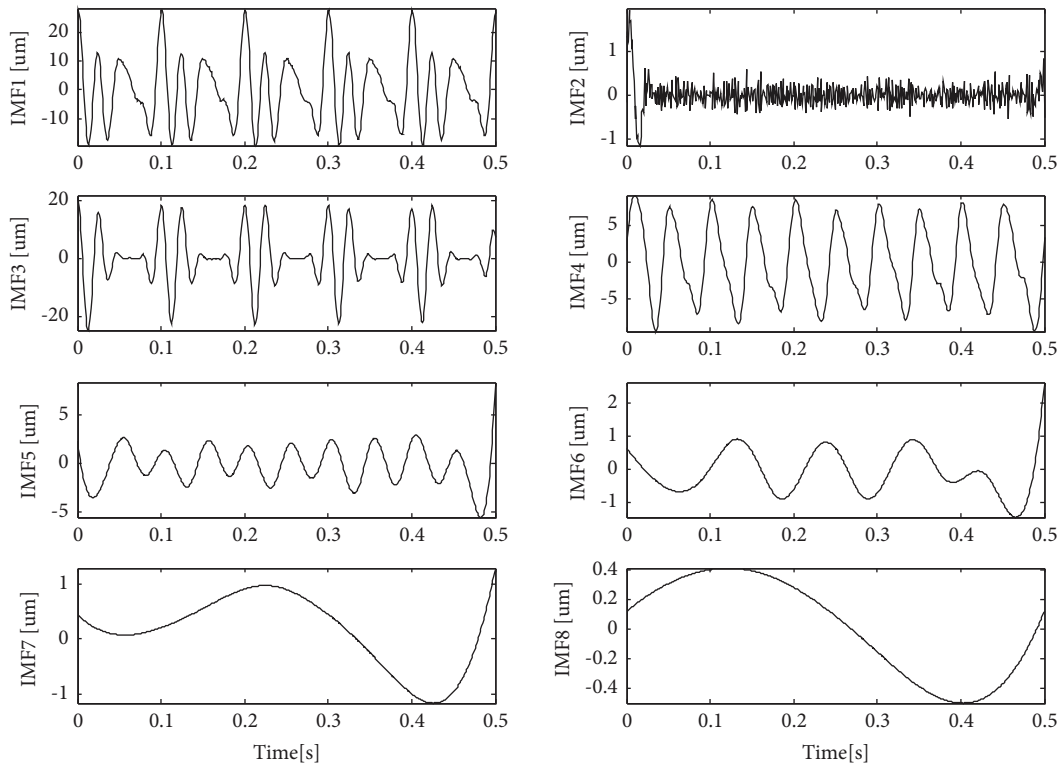


FIGURE 5: EEMD results of the observed signal in Figure 4(b).

Meanwhile, the four directions of top, down, left, and right were represented by four capital letters T , D , L , and R , respectively. The numbers are attached to the capital letters

to represent the force vectors (magnitude and direction). For example, $L2T3$ means two forces of 2 pitches and 3 pitches simultaneously applied to the left and top directions.

TABLE 3: Cosine similarities between each IMF and the mixed signal in Figure 4(a).

IMF	1	2	3	4	5	6	7	8
Sim _{cos}	0.012	0.091	0.860	0.646	0.104	0.056	0.019	0.020

TABLE 4: Cosine similarities between each IMF and the mixed signal in Figure 4(b).

IMF	1	2	3	4	5	6	7	8
Sim _{cos}	0.215	0.983	0.183	0.110	0.044	0.015	0.004	0.014

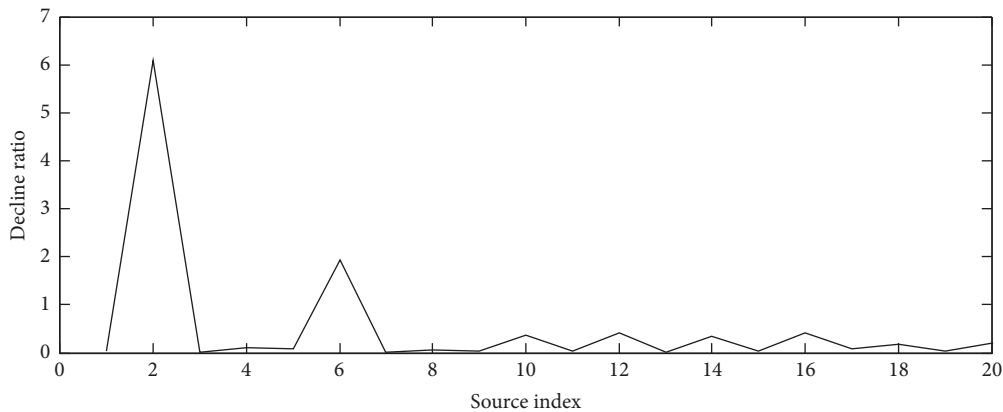


FIGURE 6: Changes of decline ratio with source index.

Note that, for comparison, all operating conditions, including the data collection parameters, are identical. The input rotating speed of the DC motor was approximately equal to 1000 rpm. Vibration signals were collected simultaneously using five probes. Each file of the vibration signal consisted of 2 s of data at a sampling rate of 4096 Hz. The order tracking technique was also involved in gaining vibration parameters as precisely as possible when the procedure was used to process vibration signals. Meanwhile, because rotor balancing essentially requires the phase measurement of the synchronous harmonics of the vibration signal with respect to a reference, the key phasor (one of the probes fixed near the motor) was adopted to provide the reference phase angle value associated with the filtered amplitudes measured by each transducer.

3.3.2. The Standard Rotor Balance Process. The standard rotor balance process without additional radial force was first introduced to obtain the reference parameters, such as mass unbalance vector and balancing vector corresponding to the original imbalance.

First, the peak-to-peak values and vibration vectors at 1X were extracted from the raw data and shown in Table 5.

As can be seen, the vibration information collected from different sensors is distinct from one another, even from the same rotor section. The probe with the highest amplitude was chosen for the balancing task according to the maintenance experience to achieve a better contrast.

A trial weight of 9.8 g was located at 270° (both quantity and angle were randomly chosen). Based on conventional ICM, rotor balancing results were gained under the unloaded condition, which inferred that only mass unbalance failures were artificially concerned regardless of the mechanical assembly errors. Note that here the mass unbalance that can be treated as the inherent failure of the rotor system persisted through the whole duration.

3.3.3. Rotor Balance Process with External Force Interference.

In practical experiments, a serial of experimental investigations have been established under different loading conditions. Considering the limit of the paper, only the condition with an additional T5R6 force was engaged to demonstrate the superior performance of the BSS-ICM algorithm. Moreover, in contrast to the previous analysis using the probe with the highest amplitude, all vibration signals were referred to the signal source to be analysed. Because there are two groups of orthogonally installed probes, the two raw signals were selected by the magnitude level. Herein, raw signals collected from 3# and 4# sensors were selected according to the magnitude. Corresponding waveforms of these two signals are described in Figure 9.

According to the algorithm flow, EEMD was used to process the selected raw signals to obtain the IMFs. Particularly, EEMD results extracted from the 3rd probe are representatively illustrated in Figure 10.

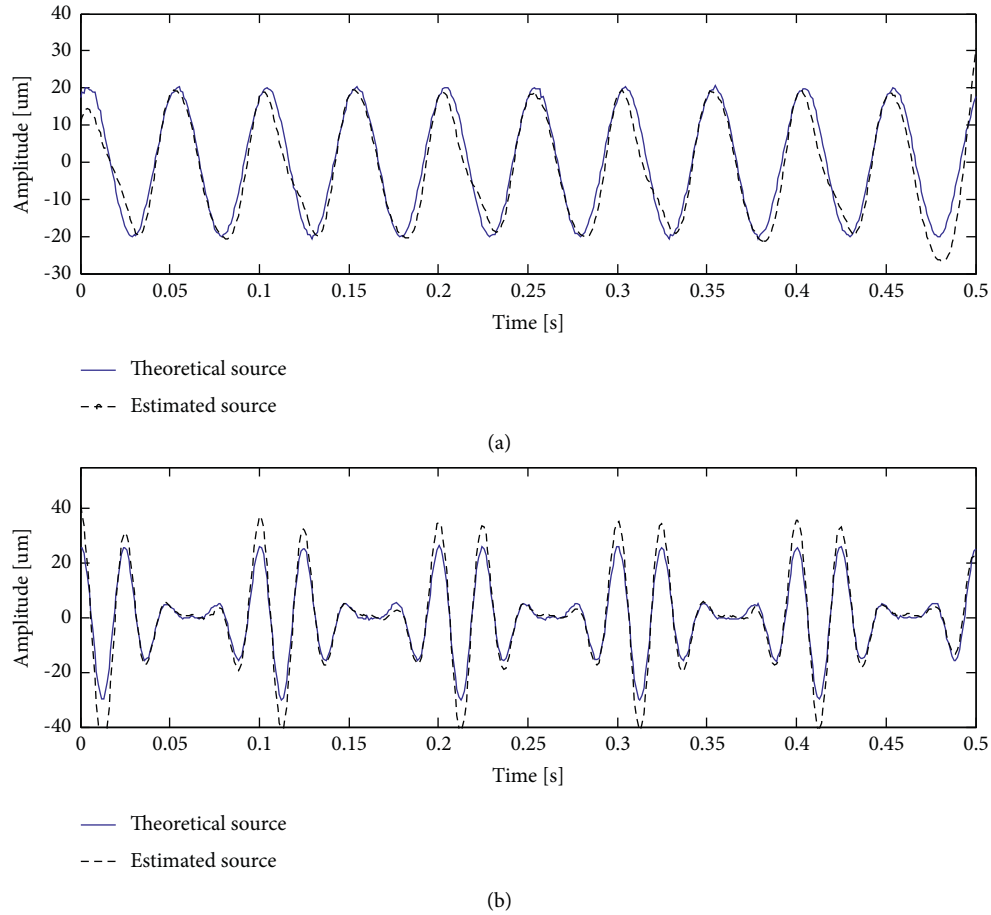


FIGURE 7: Source estimations using the proposed method.

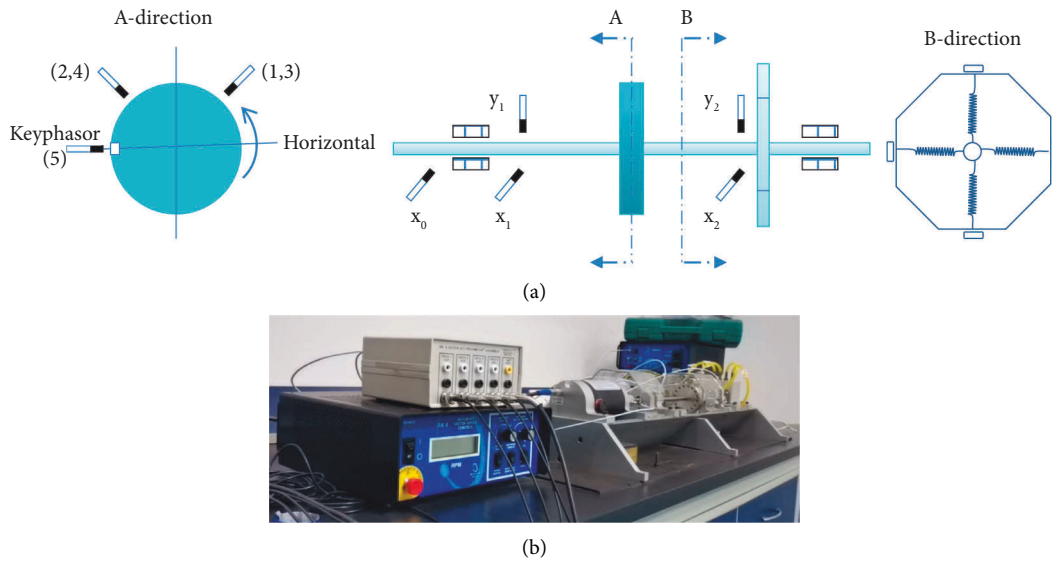


FIGURE 8: Bently Nevada Rotor Kit with a specific force loading device. (a) The structure chart and (b) the physical view.

Thereafter, the similarity between each IMF and the original vibration is computed using (11) to capture the most representative IMF. Together with the original signal, herein, the IMF

with the most significant similarity (IMF4 owns the highest values in each group) is employed to form the mixing matrix for fault number determination and blind source separation.

TABLE 5: Vibration vectors of raw signals.

Probes	1st	2nd	3rd	4th
Peak-to-peak value μm	42.1	53.0	112.0	70.0
1X vector $\mu\text{m}\angle^\circ$	36.2\angle 347	51.2\angle 79	104\angle 340	69.9\angle 76

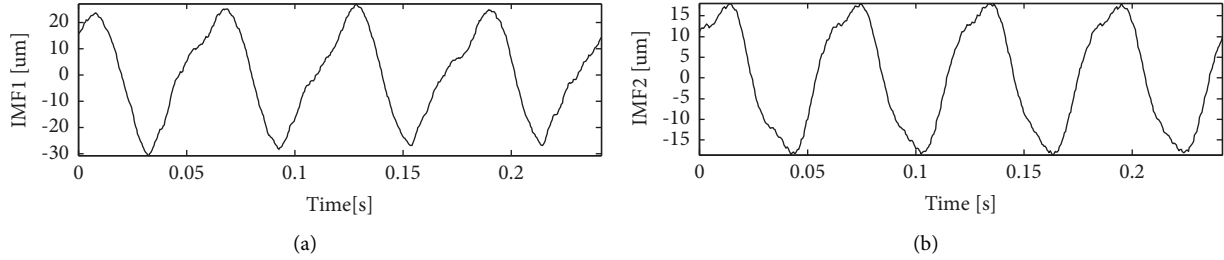


FIGURE 9: The original signal collected from (a) the 3# and (b) 4# sensors.

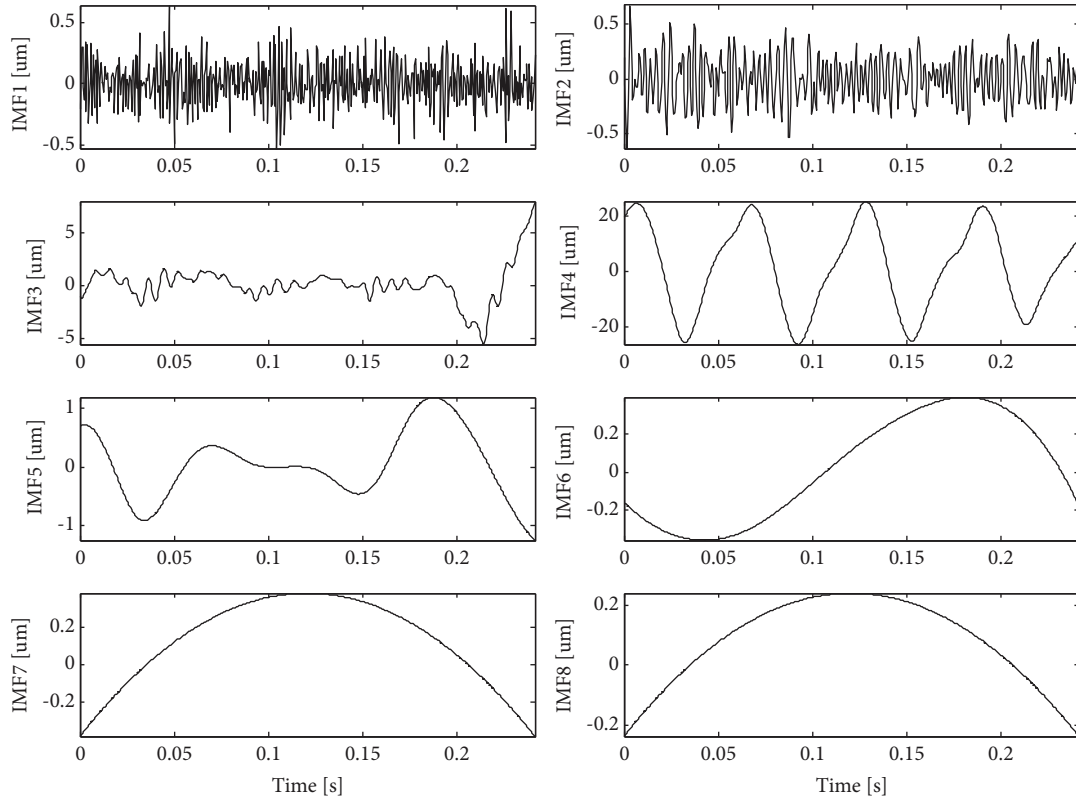


FIGURE 10: First eight IMFs of the 3rd vibration signal (from high- to low-frequency bands).

TABLE 6: Results of cosine similarities based on the first selected raw data.

IMF	1	2	3	4	5	6	7	8
Sim _{cos}	0.019	0.020	0.477	0.991	0.444	0.011	0.040	0.040

Tables 6 and 7 give the corresponding similarities of the two groups of IMFs, respectively.

Then, the SVD method is used for fault number estimation. Table 8 shows the details of the top 20 nonzero

eigenvalues related to the new observed matrix. The decline ratios are illustrated in Figure 11.

In Figure 11, it is clear that the second ratio owns the most considerable value compared to the others. In other

TABLE 7: Results of cosine similarities based on the second selected raw data.

IMF	1	2	3	4	5	6	7	8
Sim _{cos}	0.035	0.014	0.061	0.959	0.830	0.025	0.024	0.023

TABLE 8: Nonzero eigenvalues obtained by SVD.

Index	1	2	3	4	5	6	7	8	9	10
Sim _{cos}	28273	28107	4004	3459	2188	2183	1168	735	321	207
Index	11	12	13	14	15	16	17	18	19	20
Sim _{cos}	107	95	89	61	49	49	40	25	23	21

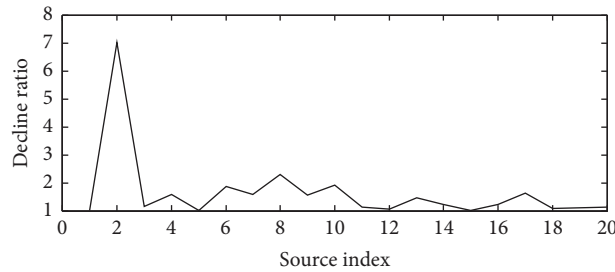


FIGURE 11: Changes of decline ratio with source index under experiment condition.

TABLE 9: Rotor balancing results using convention ICM without external force.

Run state	At condition weight (g)/angle (°)	Vibration amplitude (μm)	Phase angle (°)	External force
Original	—	104	340	—
Trial	9.8/270	51	345	—
Balanced	19/275	24.4	59	—

Final vibration amplitude reduction %: $(104-24.4)/104 = 76.54\%$.

words, the rotor system suffers from two main faults that correspond to the mass unbalance and the simulated fault generated by the external force.

Thereafter, NMF is adopted to separate the main sources from the new observed matrix, and the relationship between the decomposed signals and the two faults can be determined based on the frequency distribution. The corresponding order spectrums are introduced to obtain a much more precise balancer vector, because the order spectrum is able to eliminate the interference of the speed fluctuation.

The proposed method is validated during the whole balancing process without additional operations. Thus, the above flow involving some key steps (steps 1, 2, 4, and 5 in Section 2.4) will be repeated to obtain the corresponding vibration information under the trial condition. Note that SVD can be omitted in this case since the source number has been obtained under the original vibration situation.

Finally, once all relevant information has been obtained, ICM is employed to accomplish the rotor balancing task. Three sets of analytical results are calculated using the conventional ICM. The corresponding results are intensively elaborated in Tables 9–11.

3.3.4. Results and Discussions. According to the rotor balancing results in Tables 9–11, a brief summary can be reached. (1) Conventional ICM plays an important role in the process of rigid rotor balancing, in which the axial vibrations at 3# in cases 1 and 2 were reduced by more than 75% after field balancing. (2) The impact of the additional force is undeniable, where all amplitudes of vibrations decrease to a slighter level under the external radial force. (3) Significant changes are seen in the final balancer vectors in two cases, especially, in the correction angle, where a deviation angle of 40° is obtained. In reality, the deviation is an outrageous option. It can be easily inferred that once the external force disappears (e.g., the run-in period after the overhaul), the inappropriate installation may result in the opposite effect or uncontrollable situations like a malfunction or even fatal damage. (4) Regardless of the amplitude difference, the final balancer vector obtained by BSS-ICM in case 3 is much more effective. Compared to the referred angle in case 1, a nearly identical correction angle has been achieved, which indicates that the optimal installation position has been figured out, even if the balancing effectiveness may decline. However, the inherent balancing has been accurately modified accordingly.

TABLE 10: Rotor balancing results using convention ICM with external force.

Run state	At condition weight (g)/angle (°)	Vibration amplitude (μm)	Phase angle (°)	External force
Original	—	43	26	T5R6
Trial	4.9/135	75.8	24	T5R6
Balanced	6.5/315	8.5	129	T5R6

Final vibration amplitude reduction %: $(43-8.5)/43 = 80.23\%$. Final amplitude error of balancer vector %: $(19-6.5)/19 = 65.8\%$. Final angle error of balancer vector %: $(278-275)/275 = 14.55\%$.

TABLE 11: Rotor balancing results using BSS-ICM with external force.

Run state	At condition weight (g)/angle (°)	Vibration amplitude (μm)	Phase angle (°)	External force
Original	—	39.41	95	T5R6
Trial	4.9/135	50.75	104	T5R6
Balanced	14.48/278	—	—	T5R6

Final amplitude error of balancer vector %: $(19-14.48)/19 = 23.8\%$. Final angle error of balancer vector %: $(278-275)/275 = 1.09\%$.

4. Conclusions

In this paper, a hybrid method named BSS-ICM is successfully developed. In conjunction with the superiority of EEMD, SVD, and NMF, extraction and division of multiple features have been accomplished. The corresponding analysis results and conclusions are given as follows:

- (1) The hybrid method is capable of maximizing the use of the vibration information, where signals collected from different sensors are involved for further analysis.
- (2) A root dynamic balancing and implemental framework is successfully developed to accomplish the task of vibration reduction.
- (3) The effectiveness of the proposed method is verified using both numerical simulations and practical applications, in which the signal characteristics of the common rotor failure are successfully obtained and utilized for further analysis, i.e., rotor balancing.
- (4) Results of simulations and experiments indicate that the novel method has the potential ability of extracting the inherent faults from the mixed vibration signals.

Nevertheless the investigation on rotor balancing by means of BSS is still in its infancy, and modern signal processing techniques have not been sufficiently applied to this field yet, there is a slight amplitude deviation between the two balancers obtained by BSS-ICM and conventional ICM. Moreover, the final balancer vector cannot be verified because of the permission restrictions and algorithm development period, even though, based on the angle information, it still can be deduced that the calculation result meets the requirements of inherent rotor balancing.

Data Availability

The test data used to support the findings of this study are available from the corresponding author upon request.

Conflicts of Interest

The authors declare that they have no conflicts of interest.

Acknowledgments

This current work was supported by the Postdoctoral Science Foundation of China (Grant no. 2021M692603), the Natural Science Basic Research Program of Shaanxi (Grant no. 2022JM-264), and the Fundamental Research Funds for State Key Laboratory of Compressor Technology (Anhui Laboratory of Compressor Technology) (Grant nos. SKL-YSJ202106 and SKL-YSJ201907), which is highly appreciated by the authors.

References

- [1] A. M. Haidar and J. L. Palacios, "Modified ball-type Automatic balancer for rotating shafts: analysis and experiment," *Journal of Sound and Vibration*, vol. 496, Article ID 115927, 2021.
- [2] A. A. Ibraheem, N. M. Ghazaly, and G. Abdel-Jaber, "Review of rotor balancing techniques," *American Journal of Industrial Engineering*, vol. 6, pp. 19–25, 2019.
- [3] A. R. Bhende, "A new rotor balancing method using amplitude subtraction and its performance analysis with phase angle measurement-based rotor balancing method," *Australian Journal of Mechanical Engineering*, vol. 18, no. 1, pp. 112–118, 2020.
- [4] J. Wu, X. Zhang, and B. Li, "A study on vibration component separation of a rotor system during startup and its application in fault diagnosis," *Measurement Science and Technology*, vol. 30, no. 9, Article ID 095104, 2019.
- [5] G. Ranjan and R. Tiwari, "Application of active magnetic bearings for in situ flexible rotor residual balancing using a novel generalized influence coefficient method," *Inverse Problems in Science and Engineering*, vol. 27, no. 7, pp. 943–968, 2019.
- [6] R. Ye, L. Wang, X. Hou, Z. Luo, and Q. Han, "Balancing method without trial weights for rotor systems based on similitude scale model," *Frontiers of Mechanical Engineering*, vol. 13, no. 4, pp. 571–580, 2018.

- [7] S. Liu, "A modified low-speed balancing method for flexible rotors based on holospectrum," *Mechanical Systems and Signal Processing*, vol. 21, no. 1, pp. 348–364, 2007.
- [8] D. S. Alves, T. H. Machado, K. L. Cavalca, and N. Bachschmid, "Characteristics of oil film nonlinearity in bearings and its effects in rotor balancing," *Journal of Sound and Vibration*, vol. 459, Article ID 114854, 2019.
- [9] S. Singh and N. Kumar, "Combined rotor fault diagnosis in rotating machinery using empirical mode decomposition," *Journal of Mechanical Science and Technology*, vol. 28, no. 12, pp. 4869–4876, 2014.
- [10] S. Zhao, X. Ren, W. Deng, K. Lu, Y. Yang, and C. Fu, "A transient characteristic-based balancing method of rotor system without trail weights," *Mechanical Systems and Signal Processing*, vol. 148, Article ID 107117, 2021.
- [11] V. Prasad and R. Tiwari, "Identification of speed-Dependent active magnetic bearing parameters and rotor Balancing in high-speed rotor Systems," *Journal of Dynamic Systems, Measurement, and Control*, vol. 141, no. 4, 2019.
- [12] G. Ranjan and R. Tiwari, "On-site high-speed balancing of flexible rotor-bearing system using virtual trial unbalances at slow run," *International Journal of Mechanical Sciences*, vol. 183, Article ID 105786, 2020.
- [13] B. Silwal, P. Rasilo, L. Perkkiö, A. Hannukainen, T. Eirola, and A. Arkkio, "Numerical analysis of the power balance of an electrical machine with rotor eccentricity," *IEEE Transactions on Magnetics*, vol. 52, no. 3, pp. 1–4, 2016.
- [14] S. Liu and L. Qu, "A new field balancing method of rotor systems based on holospectrum and genetic algorithm," *Applied Soft Computing*, vol. 8, no. 1, pp. 446–455, 2008.
- [15] Y. Liao, G. Lang, F. Wu, and L. Qu, "An improvement to holospectrum based field balancing method by reselection of balancing object," *Journal of Vibration and Acoustics*, vol. 131, no. 3, 2009.
- [16] X. Yu, K. Mao, S. Lei, and Y. Zhu, "A new adaptive proportional-integral control strategy for rotor active balancing systems during acceleration," *Mechanism and Machine Theory*, vol. 136, pp. 105–121, 2019.
- [17] D. J. Rodrigues, A. Champneys, M. Friswell, and R. Wilson, "Experimental investigation of a single-plane automatic balancing mechanism for a rigid rotor," *Journal of Sound and Vibration*, vol. 330, no. 3, pp. 385–403, 2011.
- [18] M. Tiwari, K. Gupta, and O. Prakash, "Dynamic response of an unbalanced rotor supported on ball bearings," *Journal of Sound and Vibration*, vol. 238, no. 5, pp. 757–779, 2000.
- [19] B. Li, C. Xie, B. Lang, S. Lu, and X. Zhang, "Effect analysis of rotor balancing under conditions of external forces," *Presented at the the 5th International Conference on Robotics, Control and Automation*, Seoul, 2021.
- [20] C. Y. Yu, Y. Li, B. Fei, and W. L. Li, "Blind source separation based x-ray image denoising from an image sequence," *Review of Scientific Instruments*, vol. 86, no. 9, pp. 093701–093771, 2015.
- [21] J. Wodecki, P. Kruczek, A. Bartkowiak, R. Zimroz, and A. Wylomańska, "Novel method of informative frequency band selection for vibration signal using Nonnegative Matrix Factorization of spectrogram matrix," *Mechanical Systems and Signal Processing*, vol. 130, pp. 585–596, 2019.
- [22] P. O. Hoyer, "Non-negative matrix factorization with sparseness constraints," *Journal of Machine Learning Research*, vol. 5, 2004.
- [23] Y.-s. Yang, A.-b. Ming, Y.-y. Zhang, and Y.-s. Zhu, "Discriminative non-negative matrix factorization (DNMF) and its application to the fault diagnosis of diesel engine," *Mechanical Systems and Signal Processing*, vol. 95, pp. 158–171, 2017.
- [24] B. Li, X. Zhang, and J. Wu, "New procedure for gear fault detection and diagnosis using instantaneous angular speed," *Mechanical Systems and Signal Processing*, vol. 85, pp. 415–428, 2017.
- [25] Z. Wu and N. E. Huang, "Ensemble empirical mode decomposition: a noise-assisted data analysis method," *Advances in Adaptive Data Analysis*, vol. 1, no. 1, pp. 1–41, 2009.
- [26] F. Jiang, Z. Zhu, W. Li, G. Chen, and G. Zhou, "Robust condition monitoring and fault diagnosis of rolling element bearings using improved EEMD and statistical features," *Measurement Science and Technology*, vol. 25, no. 2, Article ID 025003, 2013.
- [27] Y. Lei, Z. He, and Y. Zi, "Application of the EEMD method to rotor fault diagnosis of rotating machinery," *Mechanical Systems and Signal Processing*, vol. 23, no. 4, pp. 1327–1338, 2009.
- [28] S. Zhou, S. W. Dyer, K.-k. Shin, J. Shi, and J. Ni, "Extended influence coefficient method for rotor active balancing during acceleration," *Journal of Dynamic Systems, Measurement, and Control*, vol. 126, no. 1, pp. 219–223, 2004.